EARTHQUAKE SPECTRA

The Professional Journal of the Earthquake Engineering Research Institute

PREPRINT

This preprint is a PDF of a manuscript that has been accepted for publication in *Earthquake Spectra*. It is the final version that was uploaded and approved by the author(s). While the paper has been through the usual rigorous peer review process for the Journal, it has not been copyedited, nor have the figures and tables been modified for final publication. Please also note that the paper may refer to online Appendices that are not yet available.

We have posted this preliminary version of the manuscript online in the interest of making the scientific findings available for distribution and citation as quickly as possible following acceptance. However, readers should be aware that the final, published version will look different from this version and may also have some differences in content.

The DOI for this manuscript and the correct format for citing the paper are given at the top of the online (html) abstract.

Once the final, published version of this paper is posted online, it will replace the preliminary version at the specified DOI.

Development of a Fragility Model for the Residential Building Stock in South America

Mabé Villar-Vega[a)], Vitor Silva [a)b)], M.EERI, Helen Crowley[a)1c)], M.EERI, Catalina Yepes[a)], M.EERI , Nicola Tarque[a)], Ana Beatriz Acevedo[a)], Matías A. Hube[a)] ,M.EERI , Gustavo Coronel D.[a)], Hernán Santa María[f)]

South America, and in particular the Andean countries are exposed to high levels of seismic hazard, which, when combined with the elevated concentration of population and properties, has led to an alarming potential for human and economic losses. Although several fragility models have been developed in recent decades for South America, and occasionally used in probabilistic risk analysis, these models have been developed using distinct methodologies and assumptions, which renders any direct comparison of the results across countries questionable, and thus application at a regional level unreliable. This publication aims at obtaining a uniform fragility model for the most representative building classes in the Andean region, for large-scale risk analysis. To this end, sets of single-degree-of-freedom oscillators were created and subjected to a series of ground motion records using non-linear time history analyses, and the resulting damage distributions were used to derive sets of fragility functions.

INTRODUCTION

A large portion of the South American territory, and in particular the Andean countries (Argentina, Bolivia, Chile, Colombia, Ecuador, Peru, and Venezuela), is subjected to damaging

[a)] GEM Foundation, Pavia, Italy
[b)] RISCO, Department of Civil Engineering, University of Aveiro, Aveiro, Portugal
[c)] European Centre for Training and Research in Earthquake Engineering, EUCENTRE, Pavia, Italy
[d)] Department of Engineering, Pontificia Universidad Católica del Perú, Lima, Perú
[e)] EAFIT University, Medellin, Colombia
[f)] Pontificia Universidad Católica de Chile and National Research Center for Integrated Natural Disaster Management CONICYT/FONDAP/15110017, Santiago, Chile
[g)] IMME-UCV and FUNVISIS, Caracas, Venezuela

earthquakes (e.g. Pisco-Peru 2007, Maule-Chile 2010). In the last two decades alone, over 3000 fatalities have been reported, and economic losses have exceeded 30 billion USD. According to Jaiswal *et al*. (2014), approximately 35% of the population in South America resides in areas of moderate or high seismic hazard. In addition, in less urbanized regions, poor construction technologies, use of weak materials, and inadequate enforcement of seismic regulations have led to a high seismic vulnerability in the built-up environment. This concentration of population, livelihood, and physical infrastructure in hazard-prone areas has led to a considerable level of seismic risk in the Andean countries. In order to improve the understanding of seismic hazard and risk in South America, the Global Earthquake Model (GEM) led a regional programme (SARA - South America Risk Assessment project) to develop uniform models and datasets, in collaboration with local experts. These results have been employed to profile the earthquake risk in the Andean countries. The study presented herein covered the fragility assessment of the residential building stock.

Earthquake risk assessment is a fundamental step for the creation and implementation of disaster risk reduction (DRR) measures. This can include the development of retrofitting/strengthening campaigns, creation of financial mechanisms to transfer the risk from local governments to the private sector, planning of urban or regional pre- and post-disaster emergency plans, or definition of regulations to endorse seismic-proof construction practices (Silva *et al*. 2014a). The development of earthquake risk models requires three main components: a probabilistic seismic hazard model, an exposure model containing the location and value of the elements exposed to the hazard (e.g. buildings, population), and a set of vulnerability functions establishing the likelihood of loss conditional on a ground shaking level. Fragility functions which establish the probability of exceeding a set of damage states conditional on ground shaking are also commonly used in earthquake risk analysis.

The structural/physical vulnerability of the South American building stock has been the target of several studies, as presented in the following section. These studies focused on the employment of analytical methodologies for the evaluation of the seismic response of a single structure (or a class of buildings), which was combined with a damage model in order to derive sets of fragility functions (e.g. Bonett 2003, Tarque *et al*. 2012, Haindl *et al*. 2015) for different seismic performance levels. Despite the existence of these models for South America, there are a number of issues that prevent their employment in large-scale probabilistic seismic risk analysis. For example, the derivation methodologies, structural modelling assumptions, and

damage criteria adopted by each study are often very different, which renders any direct comparison of limited validity. The number and type of damage states also varies considerably across the existing models. For example, Tarque (2008) adopted three damage states for Peruvian earthen dwellings, whilst Rojas (2010) preferred four damage states for the fragility assessment of buildings in Venezuela, and Haindl *et al.* (2015) used only the collapse limit state for reinforced concrete shear wall houses in Chile. Some of the existing models have been developed for specific structures, and not for classes of buildings. Furthermore, a number of fragility functions have been developed using macroseismic intensity (e.g. Safina, 2003), which is usually useful for the assessment of damage from single seismic events (scenario analysis), but less convenient for the calculation of probabilistic risk, due to the lack of seismic hazard models or datasets using this intensity measure. Finally, it is worth noting that there are still certain types of construction (e.g. stone masonry) whose structural vulnerability has not yet been investigated. These factors demonstrate the need to develop a uniform fragility model capable of overcoming these issues.

In the study presented herein, a comprehensive literature review has been performed to investigate the main structural and dynamic characteristics of the South American building stock, which were used to develop single-degree-of-freedom oscillators. These models were tested against sets of ground motion records using nonlinear dynamic analyses, and the resulting damage distribution was employed to derive sets of fragility functions. The results of this study are useful for regional and national earthquake risk analyses, but less appropriate for city-level scenarios or local risk analyses. For the latter type of calculations, models with a higher level of detail and considering the local characteristics of the building portfolio should be employed, such as those described in the following section.

REVIEW OF EXISTING MODELS FOR THE ANDEAN REGION

This section describes several studies that were relevant for the development of the methodology and definition of the structural parameters considered in this study. For the sake of simplicity and brevity, only studies for Chile, Colombia, Peru and Venezuela are presented given their high levels of seismic hazard.

CHILE

In Chile, Martínez (2012) developed damage probability matrices (DPM) and fragility functions for reinforced concrete (RC) structures. Six typologies were defined, which included

low-, mid-, and high-rise RC frame and wall buildings. For each of them, a pushover analysis was performed and the resulting capacity curve was compared to the demand spectrum from the Chilean seismic code. The damage thresholds were defined based on the results of the Risk-UE project (Milutinovic and Trendafiloski, 2003). Haindl et al. (2015) developed fragility curves for a reinforced concrete shear wall house using incremental dynamic analysis and following FEMA P-695 (FEMA, 2009) procedure. Tapia et al. (2002) performed a seismic vulnerability assessment for structures located in the northern region of Chile, including the cities of Antofagasta, Arica, and Copiapó. In this study, a set of vulnerability functions was developed for the most common building classes, including reinforced concrete, masonry, and adobe. These vulnerability functions were adapted from an existing set of curves that had been developed for Santiago, using damage data from the 1985 Algarrobo earthquake.

COLOMBIA

In the case of Colombia, vulnerability functions have been developed for RC wall systems (Maldonado et al., 2010), rammed earth (*tapia*) structures (Maldonado and Chio Cho, 2009), and low-rise unreinforced masonry buildings (Gómez and Rodríguez, 2006). In the first two cases, the expected seismic performance was assigned by expert opinion while in the latter, a numerical simulation was performed to define a hypothetical sample of structures, based on higher and lower bounds for the each structural parameter of interest. Salgado-Gálvez et al. (2014) developed vulnerability functions for 35 building classes within a fully probabilistic risk assessment study developed for the city of Medellín. Bonett (2003) has also calculated fragility functions for mid- and high-rise RC frames based on non-linear time history analyses (NLTHA). In this study, two ductility levels were considered in order to cover structures both with and without seismic provisions.

PERU

Among the existing models for Peru, Tarque *et al*. (2012) developed analytical fragility functions for adobe dwellings in Cusco, considering in- and out-of-plane failure. This study employed the Displacement-based Earthquake Loss Assessment (DBELA - Crowley et al. 2004b) approach to compare the capacity of the walls with the corresponding displacement response spectra. Velásquez (2006) generated analytical fragility functions for typical Peruvian high-school buildings (i.e. RC frames with masonry infills). In this case, NLTHA using synthetic accelerograms were used to calculate the structural response, and derive sets of fragility functions. These functions were used in loss estimations for three different earthquake

scenarios. Additionally, RC wall buildings have been studied by Delgado and Rodríguez (2006) and Quiroz and Maruyama (2013 and 2014). In the former case, fragility functions for mid-rise buildings with limited ductility were derived based on the judgement of several experts. In the latter studies, analytical fragility functions for mid-rise buildings with thin walls were developed using NLTHA with sets of ground motion records from a number of different countries (including Peru, Chile, and the United States).

VENEZUELA

In Venezuela, Rojas (2010) developed a set of analytical fragility functions for six different RC frame buildings with variable age, number of storeys and occupancy, considering the variability in some of the structural and geometrical properties. Rojas and Coronel (2014) developed fragility and vulnerability functions for residential RC frame buildings based on pushover analyses, while Vielma *et al*. (2014) used incremental dynamic analyses to develop fragility functions of two RC frame buildings. Safina (2003) developed fragility functions for the 20 most representative building classes in Caracas. These curves were based on the six basic vulnerability classes defined by the European Macroseismic Scale (EMS-98). In another study, analytical fragility functions for nine real RC buildings in Caracas were calculated by Safina *et al*. (2008). In this case, a non-linear static procedure was employed to obtain the response of each structure, whose results were utilized for fragility derivation. Finally, Olbrich (2015) developed fragility curves of old brick masonry structures using nonlinear analyses.

BUILDING STOCK IN SOUTH AMERICA

The building classes for the Andean countries presented herein were defined by the regional exposure model developed within the SARA project (Yepes *et al*. 2015). This exposure model was based on the information provided by each of the national population and housing census surveys, local experts' judgement, information from the World Housing Encyclopedia (WHE), and the Global Exposure Database (GED) of the Global Earthquake Model (Gamba, 2014). Figure 1 illustrates the distribution of the residential building stock according to the most common construction materials (M – brick masonry, CR – reinforced concrete, ER/ADO – earthen or adobe, W – wooden, UNK – unknown, MUR+ST – stone masonry) in the Andean region according to Yepes *et al.* (2015).

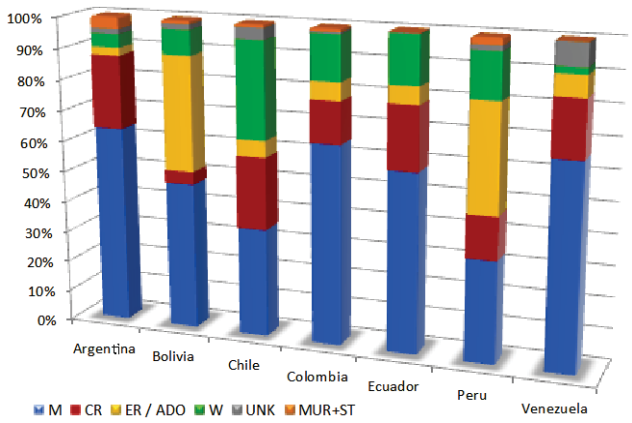

Figure 1. Distribution of the residential building stock according to the most common construction materials in the Andean countries.

As presented in Figure 1, masonry is the most common construction material in the Andean countries, representing more than half of the total number of buildings. Reinforced concrete and earthen/adobe materials are also commonly used in South America, the latter being used especially in Bolivia and Peru. The "Unknown" category corresponds to informal (non-engineered) construction, made mostly with light wooden elements. These macro-building classes have been further divided according to the expected level of ductility (associated with a design code level) and a number of storeys. Table 1 depicts the resulting building classes categorised according to the GEM Building Taxonomy (Brzev et al., 2013). A complete description of each of these systems can be found in Yepes et al. (2015).

METHODOLOGY FOR THE DERIVATION OF FRAGILITY FUNCTIONS

The Global Earthquake Model has supported the creation of guidelines for the development of empirical and analytical fragility functions (Rossetto et al. 2013; D'Ayala et al. 2014). These documents describe the most common fragility methodologies and provide recommendations regarding which approach should be followed based on the required level of complexity and data availability.

In this study, the structural capacity of each building class was represented by a large number of equivalent single-degree-of-freedom (SDOF) oscillators (thus enabling the propagation of the building-to-building variability), and the seismic demand by over 300 ground motion records (in order to consider the record-to-record variability). These two components were combined through a series NLTHA, leading to a distribution of damage conditional on a level of seismic intensity. This section describes how each one of these

components has been defined, as well as the various steps comprising the fragility methodology.

Table 1. Most common building classes in the Andean region, based on Yepes et al. (2015)

GEM Taxonomy	Typology description
CR/LDUAL/H:10	Reinforced concrete dual frame-wall system, 10 storeys
CR/LFINF/DUC/H:1	Reinforced concrete infilled frame, ductile, 1 storey
CR/LFINF/DUC/H:3	Reinforced concrete infilled frame, ductile, 3 storeys
CR/LFINF/DUC/H:7	Reinforced concrete infilled frame, ductile, 7 storeys
CR/LFINF/DNO/H:1	Reinforced concrete infilled frame, non-ductile, 1 storey
CR/LFINF/DNO/H:3	Reinforced concrete infilled frame, non-ductile, 3 storeys
CR/LFINF/DNO/H:7	Reinforced concrete infilled frame, non-ductile, 7 storeys
CR/LFM/DUC/H:1	Reinforced concrete moment frame, ductile, 1 storey
CR/LFM/DUC/H:2	Reinforced concrete moment frame, ductile, 2 storeys
CR/LFM/DUC/H:3	Reinforced concrete moment frame, ductile, 3 storeys
CR/LFM/DUC/H:4	Reinforced concrete moment frame, ductile, 4 storeys
CR/LFM/DUC/H:5	Reinforced concrete moment frame, ductile, 5 storeys
CR/LFM/DUC/H:6	Reinforced concrete moment frame, ductile, 6 storeys
CR/LFM/DUC/H:7	Reinforced concrete moment frame, ductile, 7 storeys
CR/LFM/DNO/H:1	Reinforced concrete moment frame, ductile, 1 storey
CR/LFM/DNO/H:2	Reinforced concrete moment frame, non-ductile, 2 storeys
CR/LFM/DNO/H:3	Reinforced concrete moment frame, non-ductile, 3 storeys
CR/LFM/DNO/H:4	Reinforced concrete moment frame, non-ductile, 4 storeys
CR/LFM/DNO/H:5	Reinforced concrete moment frame, non-ductile, 5 storeys
CR/LFM/DNO/H:6	Reinforced concrete moment frame, non-ductile, 6 storeys
CR/LFM/DNO/H:7	Reinforced concrete moment frame, non-ductile, 7 storeys
CR/LWAL/H:5	Reinforced concrete wall system, 5 storeys
CR/LWAL/H:6	Reinforced concrete wall system, 6 storeys
CR/LWAL/H:7	Reinforced concrete wall system, 7 storeys
CR/LWAL/H:8	Reinforced concrete wall system, 8 storeys
CR/LWAL/H:9	Reinforced concrete wall system, 9 storeys
CR/LWAL/H:10	Reinforced concrete wall system, 10 storeys
MCF/DUC/H:2	Confined masonry, ductile, 2 storeys
MCF/DUC/H:3	Confined masonry, ductile, 3 storeys
MCF/DNO/H:2	Confined masonry, non-ductile, 2 storeys
MCF/DNO/H:3	Confined masonry, non-ductile, 3 storeys
MUR/H:1	Unreinforced masonry, 1 storey
MUR/H:2	Unreinforced masonry, 2 storeys
MUR/H:3	Unreinforced masonry, 3 storeys
MUR+ADO/H:1	Unreinforced masonry with adobe blocks, 1 storey
MUR+ADO/H:2	Unreinforced masonry with adobe blocks, 2 storeys
MUR+ST99/H:1	Unreinforced stone masonry, 1 storey
MUR+ST99/H:2	Unreinforced stone masonry, 2 storeys
W+WLI/H:1	Light wood members, 1 storey
W+WLI/H:2	Light wood members, 2 storeys
UNK	Unknown (insufficient information available)

DERIVATION OF THE CAPACITY CURVES

In addition to the literature review previously presented, other studies were considered in order to understand the structural characteristics of each building class (e.g. Calvi 1999, Borzi et al. 2008, Ahmad *et al*. 2011). Moreover, the development of two workshops in Medellin (Colombia) and Lima (Peru) in 2014 and 2015 allowed to incorporate the opinion of several

local experts For each building class, several parameters were defined, such as the elastic and yielding period of vibration, the storey height, modal participation factor (as defined in ATC-40, 1996), number of storeys, and global drifts for the yielding and collapse damage states. The values assumed for each building class, and the studies that supported this decision, are described in Table 2. In all cases, the yield and ultimate drifts were determined based on existing damage state definitions (e.g. Calvi, 1999; Ghobarah, 2004; Tarque *et al*., 2012). These damage states have as well been defined in terms of global (or roof) drift. The values of interstorey height for all masonry classes were increased by 0.20 m from the typical values presented in literature (e.g. Tarque *et al*. 2012; Quintanilla and Ruiz, 2011) to ensure that it would be a floor-to-floor (or floor-to-roof) height instead of a floor-to-ceiling height. In the case of the "Unknown" (UNK) building class, the drift values were reduced from those of wooden systems in order to account for the usage of poor materials and inadequate practices.

Table 2. Structural information used to derive the capacity curves.

Typology	Storeys	Interstorey height (m)	Yield period (s)*	Yield drift (%)	Ultimate drift (%)	Base studies
MUR+ADO	1	2.60	0.055H	0.12	0.60	Tarque *et al.* (2012).
MUR+ADO	2	2.60	0.055H	0.10	0.55	Tarque *et al*. (2012).
MUR	1-3	2.60	$0.062H^{0.87}$	0.17	0.60	Bal *et al.* (2010), Borzi *et al.* (2008).
MUR+ST	1-2	2.60	$2*0.041H^{0.75}$	0.15	0.65	Elastic period based on Ahmad *et al.* (2011), Borzi *et al.* (2008)
LFM/DUC	1-7	2.80	0.07H	0.91	4.00	Crowley & Pinho (2006), Calvi (1999).
LFM/DNO	1-7	2.80	0.1H	0.66	2.61	Crowley & Pinho (2004a), Calvi (1999).
LFM/DNO/SOS	1-7	2.80	0.1H	0.66	1.30	Crowley & Pinho (2004a), Calvi (1999).
LWAL	5-10	2.80	2*(0.049*N)	0.80	2.00	Elastic period based on Oliveira & Navarro (2009), Ghobarah (2004).
LFINF/DUC	1-3	2.80	0.042H	0.40	1.90	Silva et al. (2013), Bal *et al.* (2010), Erberik (2007).
LFINF/DUC	4-7	2.80	0.042H	0.40	1.60	Silva et al. (2013), Bal *et al.* (2010), Erberik (2007).
LFINF/DNO	1-7	2.80	0.06H	0.36	0.80	Crowley & Pinho (2006), Bal *et al.* (2010).
MCF/DUC	1	2.60	0.042H	0.32	1.20	Silva et al. (2013), Bal *et al.* (2010).
MCF/DUC	2-3	2.60	0.042H	0.36	1.20	Silva et al. (2013), Bal *et al.* (2010).
MCF/DNO	1-3	2.60	0.05H	0.30	0.80	Crowley & Pinho (2006), Bal *et al.* (2008).
W+WLI	1-2	2.44	$2*0.0323H^{0.54}$	1.00	2.50	Camelo, V. (2003), Dolan, J. (1989), Vásquez *et al.* (2012), Goda (2014).
UNK	1	2.40	$2*0.0323H^{0.54}$	0.50	1.75	Period of vibration based on a wooden typology, and drifts defined through expert judgement.

* H – Height of the structure in meters (except for W+WLI: H - height in feet), N – Number of storeys.

Using the data from Table 2, a capacity curve (in terms of spectral acceleration - S_a versus spectral displacement - S_d) was derived assuming an elastic-perfectly plastic behaviour, according to the following expressions:

$$S_d = \frac{N_{storeys} \times h_{storey} \times \theta_{global}}{\Gamma} \quad (1)$$

$$S_{a_y} = S_{dy}\left(\frac{2\pi}{T_y}\right)^2 \quad \text{and} \quad S_{a_u} = S_{a_y} \quad (2)$$

Where S_d represents the spectral displacement at the yielding or ultimate points, depending on the global drift θ_{global}, $N_{storeys}$ stands for the number of storeys, h_{storey} refers to the inter-storey height, and Γ represents the first mode of vibration participation factor. S_{a_y} and S_{a_u} represent the spectral acceleration at the yielding and ultimate points, respectively, and T_y stands for the period of vibration at the yielding point. It is acknowledged that Equation (1) is only valid when the first mode of vibration dominates the roof drift. However, since the structures were assumed as regular and with a limited amount of storeys (less than 10), this assumption was deemed acceptable.

In the case of non-ductile reinforced-concrete moment-resisting frames, two failure mechanisms were considered: distributed damage or beam sway (LFM/DNO) and soft-storey or column sway (LFM/DNO/SOS), following the recommendations from Calvi (1999). The difference in the displacement profile between both schemes is reflected in the ultimate spectral displacement (see Table 2). Ductile frames were assumed to display only a distributed-damage failure mode, as a consequence of the seismic design provisions.

For concrete frames with infills (LFINF) and confined masonry (MCF), due to the interaction between the reinforced concrete and the masonry elements, a tri-linear model was assumed, following the recommendations by Bal *et al*. (2010) and Silva *et al*. (2014a). This model allows the prominent decrease in the strength and stiffness due to the structural degradation of the masonry walls to be taken into consideration, as illustrated in Figure 2. The same procedure explained previously for elastic-perfectly plastic curves was used to calculate the peak of the tri-linear curve, which corresponds to the yield strength of the system considering the masonry infill (either LFINF or MCF). The point from which the infill contribution remains constant (Δ_2) corresponds to the yielding point of the "bare frame" (i.e. the concrete frame alone, without any contribution of the infills), and the last point corresponds

to the ultimate displacement of the system (Δ_3). The displacements for these building classes were defined based on the yield and ultimate displacements of a bare frame. Once these values (the displacements of the bare frame) were estimated, the displacements corresponding to Δ_1 and Δ_3 (as defined in Figure 2) were calculated using the coefficients suggested by Bal *et al*. (2010), to account for the decrease in the displacement capacity of a bare frame due to the presence of infill walls. The latter study proposed a decrease of 52% for the yielding displacement and 28% for the ultimate displacement. Further details regarding the derivation of the tri-linear model can be found in Bal *et al*. (2010).

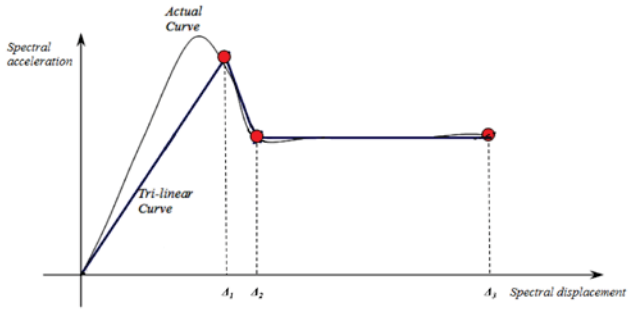

Figure 2. Tri-linear capacity curve model for RC frames with infills and confined masonry (adapted from Bal *et al.* 2010).

In order to take into consideration the building-to-building variability, it was necessary to consider a large set of capacity curves, as demonstrated by Silva *et al*. (2014b). To this end, the aforementioned capacity curve for each structure type was considered to be the median curve and a set of normally distributed curves was generated around it, taking as a reference the coefficients of variation presented by Silva *et al.* (2014b) and Borzi *et al.* (2008). These studies indicated coefficients of variation of 35% for spectral acceleration, and 24% and 41% for the yield and collapse spectral displacement, respectively. These two sources of variability were assumed as uncorrelated, and a normal distribution was adopted (e.g. Erberik 2007).

A Monte Carlo simulation was then performed in order to produce a synthetic sample of capacity curves per building class, thus allowing the propagation of this source of variability to the associated fragility model. For each building class, 150 capacity curves were generated, based on the recommendations of Silva *et al.* (2014b) to achieve convergence in the expected structural variability within a 5% tolerance. As an example, Figure 3 illustrates the results of a 4-storey ductile reinforced concrete moment-frame building (LFM/DUC/H:4) and a 2-storey ductile confined masonry structure (MCF/DUC/H:2).

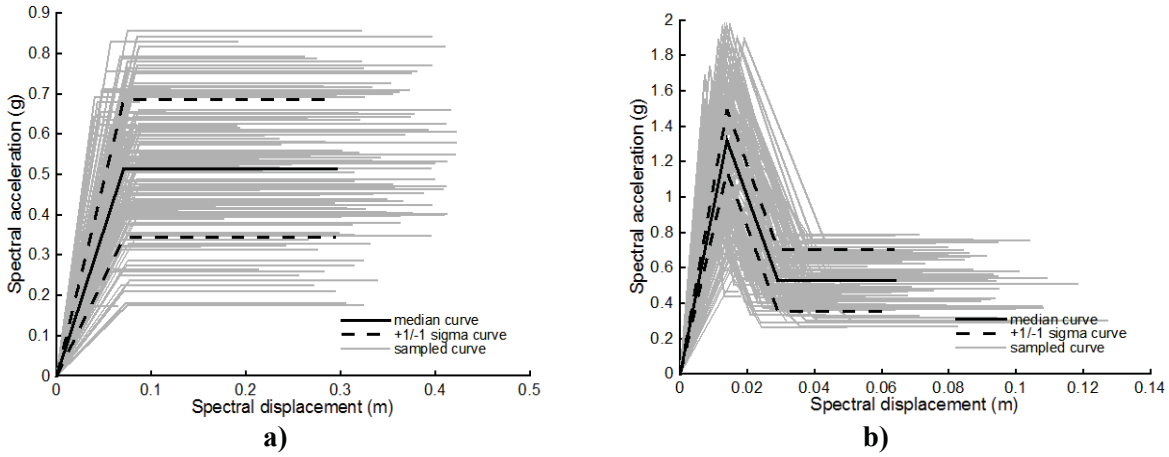

Figure 3. Median and generated capacity curves for a) LFM/DUC/H:4 and b) MCF/DUC/H:2.

Selection of Ground Motion Records

The selection of the ground motion records was performed taking into consideration the tectonic environment and seismicity in South America. Most of the seismic activity in this region involves the subduction of the Nazca and Antarctica plates beneath the South American plate. Slip along the dipping interface of these plates generates frequent and often large interplate earthquakes at depths of approximately 10 km to 60 km (Jaiswal *et al*. 2014). In addition, there are also significant events due to shallow crustal faults. For long epicentral distances (> 50 km), ground motion records with moment magnitudes between 7 and 9 were selected, while for shorter distances (≤ 50 km), records with moment magnitudes between 5 and 7 were considered. These records were selected from the PEER (Pacific Earthquake Engineering Research) database. Only rock site records were considered during the selection process, and data from recording stations at a distance below 10 km were excluded, in order to avoid near-fault effects. These records were scaled considering a range of factors between 0.5 and 2.5 (Watson-Lamprey and Abrahamson, 2006) and three intensity measure types (PGA, Sa at 0.4 s, Sa at 1.0 s), in order to have three sets of records scaled in accordance with the dynamic properties of the various building classes (from stiff low-rise structures with a short period of vibration to flexible high-rise buildings with a long period of vibration). Twelve levels of ground shaking were defined for each intensity measure type, varying from 0.05 g and 2.5 g for PGA and SA at 1.0s, and 0.05 g to 4.0 g for SA at 0.4s. These ranges of ground shaking were defined according to the minimum level expected to cause damage, and the maximum ground shaking expected in the regions with the highest seismic hazard. For each intensity measure level, 30 records were scaled at each level of ground shaking, leading to 360

ground motion records (from a total of 171 original records). The response spectra of the final set of ground motion records per intensity measure type are presented in Figure 4.

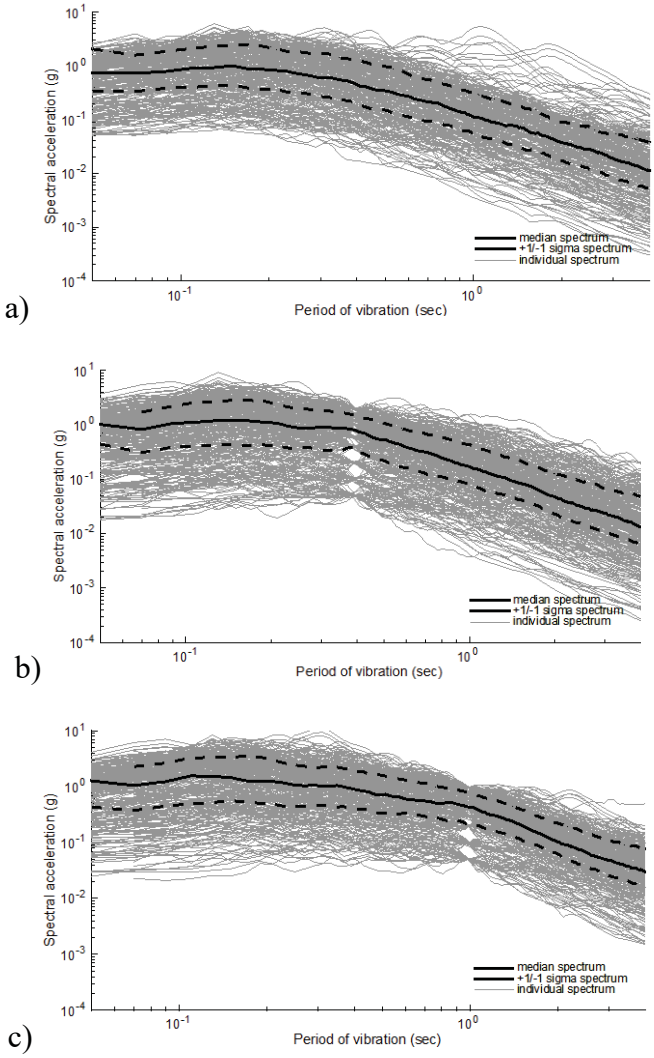

Figure 4. Response spectra for records scaled considering: a) PGA, b) Sa(0.4s), and c) Sa(1.0s).

Definition of the Damage Criterion

The definition of the damage states in this study follows closely the proposal by Lagomarsino and Giovinazzi (2006), with the exception of the second damage state (moderate damage). In the original proposal, slight damage occurs when 70% of the spectral displacement at the yielding point is exceeded (i.e. $0.7Sd_y$) and moderate damage when 150% of the same displacement is exceeded (i.e. $1.5Sd_y$). The threshold for extensive damage is defined as the mean between the yielding and the ultimate spectral displacement (i.e. $(Sd_y + Sd_u)/2$), and collapse when the ultimate displacement is exceeded (i.e. Sd_u). However, for structures with reduced ductility, the formulation for moderate and extensive limit states may lead to a

moderate damage threshold that is higher than the one for extensive damage. For this reason, the threshold for moderate damage has been defined as $0.75Sd_y + 0.25Sd_u$. This damage criteria leads to thresholds which are in agreement with several past studies (e.g. Borzi *et al*. (2008), Akkar *et al*. (2005), Silva *et al*. (2014b)). The damage criterion used herein is summarized in Table 3.

Table 3. Definition of the damage criterion.

Damage State	Damage Threshold
Slight	$0.7S_{dy}$
Moderate	$0.75S_{dy}+0.25\ S_{du}$
Extensive	$0.5(S_{dy}\ +\ S_{du})$
Collapse	S_{du}

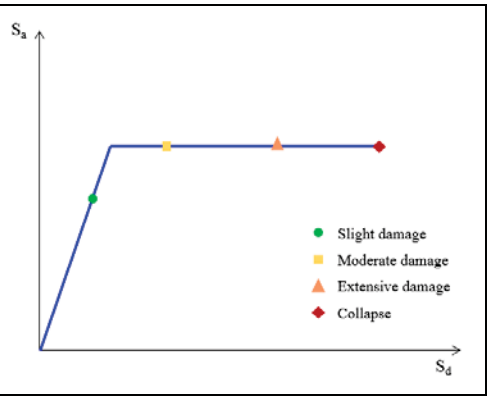

Development of fragility functions and statistical regression

The derivation of the fragility functions for each building class was performed through non-linear time history analysis (NLTHA) of SDOF systems using the GEM's Risk Modeller's Toolkit (Silva *et al.* 2015b). This module relies on the open-source software for non-linear structural analysis OpenSEES (McKenna *et al*. 2000) to perform the NLTHA on the SDOF systems. The hysteresis model of each SDOF was defined according to the associated capacity curve (i.e. a set of acceleration-displacement pairs), and using the "Pinching4 Material" model (see McKenna *et al*. (2010) for a list hysteresis models available in OpenSEES) with structural degradation in both stiffness and strength (see Figure 5). The dynamic analyses were performed with the standard pinching parameters from OpenSees, as there was not sufficient data available for a calibration process. However, as concluded by Casotto (2016) and Ibarra and Krawinkler (2005), the employment of different hysteresis features does not affect significantly the resulting fragility functions. This behaviour is due to the influence of other sources of uncertainty such as building-to-building and record-to-record variability. The definition of the various pinching parameters and how they can be calculated from a capacity curve can also be found in the OpenSees online manual.

An elastic damping of 5% was considered for the reinforced concrete structures, 10% for the masonry classes (Borzi *et al.*, 2008) and 2% for the wooden systems. The influence of

structural degradation is depicted in Figure 5, where the hysteretic curves for MCF/DUC/H:2 and LFM/DUC/H:4 are presented. Although damage degradation was considered for all of the analyses, for the sake of comparison the resulting curves without degradation are also illustrated in this figure. In each case, two hysteretic paths are presented: one where moderate damage occurred and another marked by collapse.

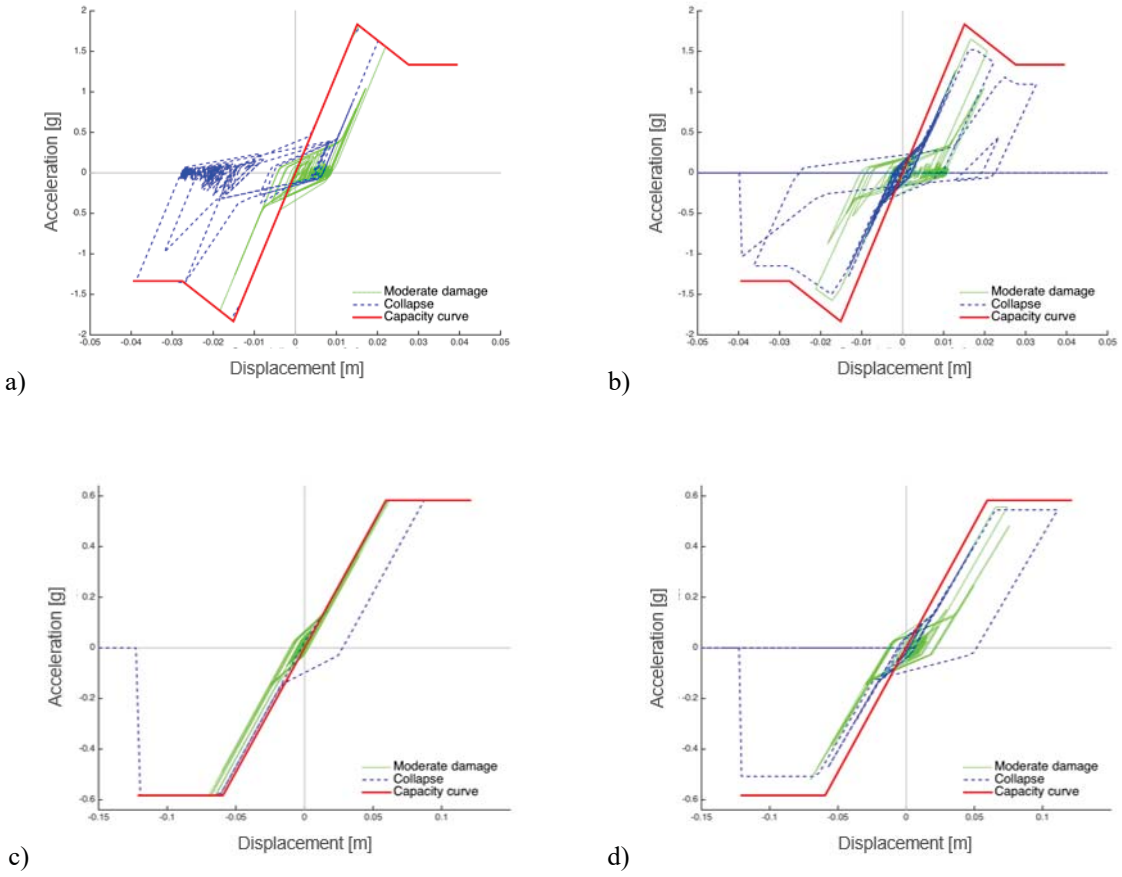

Figure 5. Hysteretic curves for a) MCF/DUC/H:2 without degradation, b) MCF/DUC/H:2 with degradation, c) LFM/DUC/H:4 without degradation, and d) LFM/DUC/H:4 with degradation.

As previously mentioned, a NLTHA was performed for each set of 150 SDOF systems (one set per building class) using the associated set of ground motion records, leading to a total of 45,000 dynamic analyses. For each SDOF, the maximum spectral displacement was computed and compared with the corresponding damage state thresholds (see Table 3) in order to allocate the structure within a damage state. This process allowed the number of SDOFs in each damage state to be calculated for each ground motion record. With this information, a damage probability matrix (DPM) was built for each building class, defining the fraction of buildings in each damage state, per ground motion record. Each record was represented by an

intensity measure type (e.g. PGA), and this distribution of ground shaking and fraction of building in each damage state was used for the derivation of the fragility curves.

Each fragility function was fitted with a cumulative probability curve with a lognormal distribution, whose statistical parameters (i.e. logarithmic mean (λ) and logarithmic standard deviation (ζ)) were calculated using the least squares method. This regression analysis was performed considering spectral acceleration for a wide range of periods of vibration, in order to understand which intensity measure type provided a better correlation with the damage distribution. This verification is presented in Figure 6a for 2-storey stone masonry (MUR+ST99/H:2), along with the resulting scatter and fragility model. In this case it can be observed that the best correlation between damage and spectral acceleration is achieved for a period of 0.4 s. In addition, Figure 6b presents the resulting scatter (i.e. the probability of reaching each damage state at each level of ground shaking) and fragility model.

This approach will naturally lead to a large number of optimal intensity measure types (one per building class). However, defining each fragility model according to a specific intensity measure type would make the seismic risk analysis quite complex and time-consuming, due to the need to generate the seismic hazard input in multiple intensity measure types. For this reason, a decision was made to consider only three intensity measure types: PGA, Sa(0.3s) and Sa(1.0s). These three intensity measure types allowed a good correlation between the damage distribution and the ground shaking, and are also the intensity measures used by the ShakeMap system of the United States Geological Survey (USGS), which increases the usability of the fragility functions derived herein.

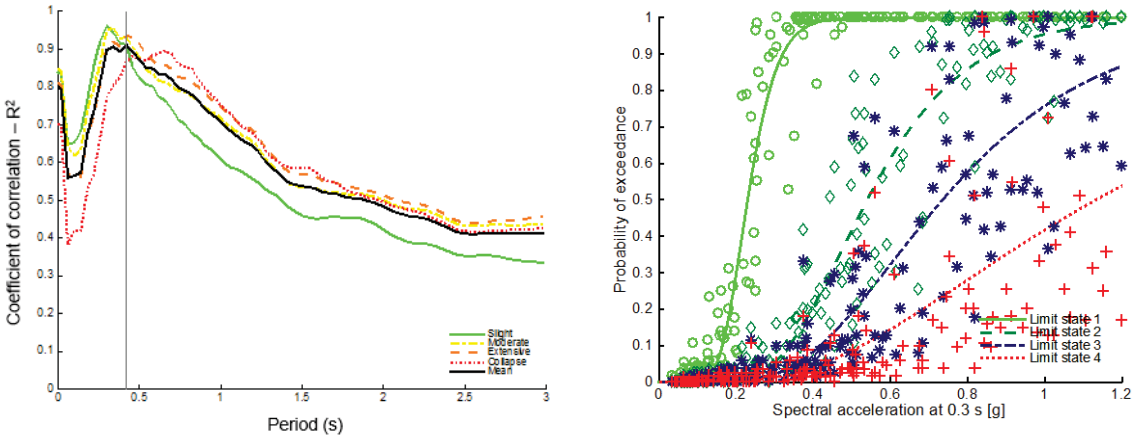

Figure 6. a) Correlation between damage and spectral acceleration; b) fragility model for MUR+ST99/H:2.

RESULTS OF THE CAPACITY AND FRAGILITY ANALYSES

Capacity Curves

Using the methodology described previously for the calculation of the structural capacity, a median capacity curve for each building class was calculated, as presented in the following tables.

Table 4. Median capacity curves for unreinforced masonry.

Typology	S_{dy}(m)	S_{du}(m)	S_{ay}(g)	S_{au}(g)
MUR+ADO/H:1	0.002	0.012	0.473	0.473
MUR+ADO/H:2	0.004	0.024	0.213	0.213
MUR/H:1	0.003	0.012	0.675	0.675
MUR/H:2	0.007	0.026	0.438	0.438
MUR/H:3	0.010	0.036	0.300	0.300
MUR+ST/H:1	0.003	0.013	0.606	0.606
MUR+ST/H:2	0.007	0.028	0.328	0.328

Table 5. Median capacity curves for RC moment-resisting frames (ductile and non-ductile) and walls.

Typology	S_{dy}(m)	S_{du}(m)		S_{ay}(g)	S_{au}(g)
		Soft Storey	Distributed Damage		
LFM/DUC/H:1	0.020	NA	0.086	2.056	2.056
LFM/DUC/H:2	0.043	NA	0.187	1.114	1.114
LFM/DUC/H:3	0.059	NA	0.258	0.685	0.685
LFM/DUC/H:4	0.077	NA	0.338	0.504	0.504
LFM/DUC/H:5	0.094	NA	0.415	0.396	0.396
LFM/DUC/H:6	0.113	NA	0.494	0.328	0.328
LFM/DUC/H:7	0.130	NA	0.572	0.279	0.279
LFM/DNO/H:1	0.014	0.057	0.056	0.731	0.731
LFM/DNO/H:2	0.031	0.077	0.122	0.396	0.396
LFM/DNO/H:3	0.043	0.101	0.168	0.244	0.244
LFM/DNO/H:4	0.056	0.116	0.220	0.179	0.179
LFM/DNO/H:5	0.069	0.130	0.270	0.141	0.141
LFM/DNO/H:6	0.082	0.145	0.322	0.116	0.116
LFM/DNO/H:7	0.095	0.160	0.373	0.099	0.099
LWAL/H:5	0.083	NA	0.207	1.391	1.391
LWAL/H:6	0.099	NA	0.247	1.151	1.151
LWAL/H:7	0.114	NA	0.286	0.979	0.979
LWAL/H:8	0.130	NA	0.325	0.851	0.851
LWAL/H:9	0.145	NA	0.363	0.751	0.751
LWAL/H:10	0.160	NA	0.400	0.671	0.671

Table 6. Median capacity curves for infilled frame and confined masonry systems (ductile and non-ductile).

Typology	$S_{dy,1}$ (m)	$S_{dy,2}$ (m)	S_{du} (m)	$S_{ay,1}$ (g)	$S_{ay,2}$ (g)	S_{au} (g)
LFINF/DUC/H:1	0.009	0.020	0.062	2.509	2.056	2.056
LFINF/DUC/H:2	0.020	0.043	0.134	1.359	1.114	1.114
LFINF/DUC/H:3	0.028	0.059	0.186	0.836	0.685	0.685
LFINF/DUC/H:4	0.037	0.077	0.243	0.615	0.504	0.504
LFINF/DUC/H:5	0.045	0.094	0.299	0.483	0.396	0.396
LFINF/DUC/H:6	0.054	0.113	0.356	0.400	0.328	0.328
LFINF/DUC/H:7	0.063	0.130	0.412	0.340	0.279	0.279
LFINF/DNO/H:1	0.007	0.014	0.040	1.106	0.731	0.731
LFINF/DNO/H:2	0.015	0.031	0.088	0.599	0.396	0.396
LFINF/DNO/H:3	0.020	0.043	0.121	0.369	0.244	0.244
LFINF/DNO/H:4	0.027	0.056	0.159	0.271	0.179	0.179
LFINF/DNO/H:5	0.033	0.069	0.195	0.213	0.141	0.141
LFINF/DNO/H:6	0.039	0.082	0.232	0.176	0.116	0.116
LFINF/DNO/H:7	0.045	0.095	0.269	0.150	0.099	0.099
MCF/DUC/H:1	0.006	0.013	0.029	2.161	0.971	0.971
MCF/DUC/H:2	0.014	0.029	0.062	1.317	0.526	0.526
MCF/DUC/H:3	0.019	0.040	0.086	0.810	0.324	0.324
MCF/DNO/H:1	0.006	0.013	0.029	1.430	0.971	0.971
MCF/DNO/H:2	0.012	0.026	0.057	0.774	0.476	0.476
MCF/DNO/H:3	0.018	0.038	0.083	0.477	0.312	0.312

Table 7. Median capacity curves for wooden and unknown typologies.

Typology	S_{dy}(m)	S_{du}(m)	S_{ay}(g)	S_{au}(g)
W+WLI/H:1	0.019	0.047	1.916	1.916
W+WLI/H:2	0.041	0.102	1.963	1.963
UNK	0.009	0.032	0.959	0.959

As described in Tables 4 to 7, low-rise buildings demonstrate higher values of spectral acceleration and lower displacements than those with a higher number of storeys. This was to be expected, as stronger and stiffer structures tend to attract higher inertial forces. In addition, it can be seen that for a given building class, non-ductile structures demonstrate lower values of spectral ordinates. These results also indicate that the unreinforced masonry classes (including adobe) exhibit the most fragile behaviour. Particularly in the case of adobe, the low values obtained for the spectral ordinates confirm the highly fragile behaviour of this material. Unreinforced masonry classes present high values of ductility (see tables 2 and 4), in some cases even larger than those obtained for ductile building classes. However, as explained by

Akkar *et al*. (2005), since ductility is the relationship between ultimate and yield displacements, very low values of the latter (due to high initial stiffness) can lead to artificially high values of ductility, even if the ultimate displacement is still a low.. This behaviour has also been observed in several past studies (e.g. Akkar *et al*., 2005, Borzi *et al*., 2008, Tarque *et al*., 2012, Varum *et al*., 2014).

Fragility Functions

This section contains the results obtained for the fragility functions (logarithmic mean (λ) and logarithmic standard deviation (ζ)) for each building class). The intensity measure type chosen for the derivation of the functions and the mean Pearson correlation coefficient (*R*) are also reported. The latter parameter describes how well the cumulative lognormal function represented the dispersion of the NLTHA results.

Table 8. Fragility functions for the masonry building classes.

Typology	IM	Damage States								Mean R
		Slight		Moderate		Extensive		Collapse		
		λ	x	λ	x	λ	x	λ	x	
MUR/H:1	PGA	-1.418	0.310	-0.709	0.328	-0.496	0.322	-0.231	0.317	0.967
MUR/H:2	Sa at 0.3 s	-1.112	0.269	-0.365	0.325	-0.088	0.372	0.288	0.513	0.956
MUR/H:3	Sa at 0.3 s	-1.189	0.338	-0.520	0.447	-0.216	0.501	0.220	0.685	0.908
MUR+ADO/H:1	PGA	-1.782	0.371	-0.894	0.326	-0.644	0.328	-0.335	0.346	0.964
MUR+ADO/H:2	Sa at 0.3 s	-1.634	0.273	-0.707	0.367	-0.371	0.447	0.092	0.610	0.938
MUR+ST99/H:1	PGA	-1.502	0.295	-0.718	0.310	-0.492	0.311	-0.215	0.322	0.965
MUR+ST99/H:2	Sa at 0.3 s	-1.270	0.279	-0.427	0.370	-0.120	0.455	0.315	0.637	0.938
MCF/H:1	PGA	-0.532	0.407	0.251	0.394	0.364	0.377	0.578	0.382	0.968
MCF/H:2	Sa at 0.3 s	-0.299	0.343	0.477	0.376	0.658	0.406	1.003	0.494	0.952
MCF/H:3	Sa at 0.3 s	-0.510	0.355	-0.307	0.434	0.551	0.513	1.002	0.656	0.920
MCF/H:1/DNO	PGA	-0.804	0.307	-0.046	0.320	0.127	0.314	0.386	0.367	0.970
MCF/H:2/DNO	Sa at 0.3 s	-0.700	0.371	0.130	0.351	0.381	0.433	0.808	0.490	0.948
MCF/H:3/DNO	Sa at 1.0 s	-2.422	0.495	-1.592	0.573	-1.189	0.587	-0.629	0.608	0.909

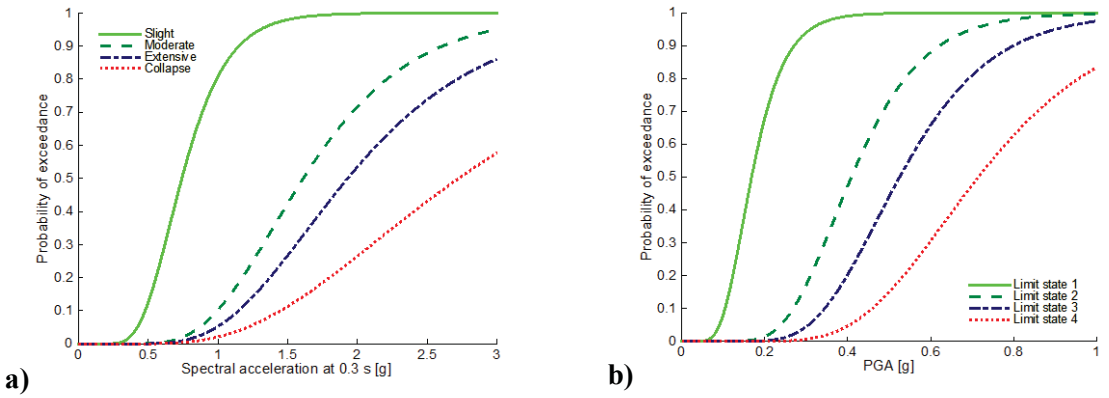

Figure 7. Fragility curves for a) MCF/DUC/H:2 and b) MUR+ADO/H:1.

Table 9. Fragility functions for reinforced concrete building classes

Typology	IM	Damage States								Mean R
		Slight		Moderate		Extensive		Collapse		
		λ	x	λ	x	λ	x	λ	x	
LFM/H:1	Sa at 0.3 s	0.088	0.348	0.919	0.398	1.179	0.381	1.616	0.507	0.920
LFM/H:2	Sa at 1.0 s	-1.786	0.535	-0.752	0.688	-0.230	0.742	0.362	0.673	0.855
LFM/H:3	Sa at 1.0 s	-1.625	0.435	-0.631	0.564	-0.194	0.572	0.329	0.590	0.914
LFM/H:4	Sa at 1.0 s	-1.257	0.327	-0.419	0.350	-0.058	0.404	0.436	0.525	0.930
LFM/H:5	Sa at 1.0 s	-1.214	0.313	-0.335	0.367	0.073	0.454	0.614	0.548	0.903
LFM/H:6	Sa at 1.0 s	-1.126	0.348	-0.251	0.446	0.171	0.546	0.737	0.693	0.883
LFM/H:7	Sa at 1.0 s	-0.997	0.420	-0.095	0.500	0.349	0.593	1.002	0.836	0.820
LFM/H:1/DNO	Sa at 0.3 s	-0.785	0.333	-0.006	0.319	0.256	0.372	0.643	0.437	0.963
LFM/H:2/DNO	Sa at 1.0 s	-2.259	0.405	-1.460	0.474	-1.058	0.477	-0.551	0.500	0.937
LFM/H:3/DNO	Sa at 1.0 s	-2.085	0.264	-1.242	0.325	-0.877	0.379	-0.380	0.453	0.973
LFM/H:4/DNO	Sa at 1.0 s	-1.841	0.292	-1.068	0.403	-0.717	0.474	-0.195	0.591	0.944
LFM/H:5/DNO	Sa at 1.0 s	-1.721	0.421	-0.882	0.521	-0.481	0.576	0.069	0.679	0.894
LFM/H:6/DNO	Sa at 1.0 s	-1.600	0.494	-0.754	0.562	-0.357	0.597	0.191	0.692	0.867
LFM/H:7/DNO	Sa at 1.0 s	-1.484	0.576	-0.635	0.646	-0.255	0.693	0.314	0.832	0.836
LFM/H:1/DNO/SOS	Sa at 0.3 s	-0.820	0.317	-0.054	0.334	0.205	0.383	0.582	0.469	0.966
LFM/H:2/DNO/SOS	Sa at 1.0 s	-2.179	0.393	-1.572	0.470	-1.308	0.498	-0.897	0.516	0.948
LFM/H:3/DNO/SOS	Sa at 1.0 s	-1.987	0.286	-1.376	0.315	-1.133	0.357	-0.752	0.441	0.984
LFM/H:4/DNO/SOS	Sa at 1.0 s	-1.715	0.342	-1.187	0.423	-0.977	0.480	-0.638	0.566	0.959
LFM/H:5/DNO/SOS	Sa at 1.0 s	-1.588	0.482	-1.059	0.547	-0.877	0.581	-0.554	0.641	0.917
LFM/H:6/DNO/SOS	Sa at 1.0 s	-1.445	0.567	-0.919	0.629	-0.767	0.653	-0.485	0.687	0.881
LFM/H:7/DNO/SOS	Sa at 1.0 s	-1.309	0.645	-0.782	0.678	-0.646	0.696	-0.386	0.739	0.852
LFINF/H:1	PGA	-0.401	0.410	0.482	0.391	0.694	0.364	0.973	0.406	0.927
LFINF/H:2	Sa at 0.3 s	-0.206	0.323	0.754	0.377	1.078	0.446	1.666	0.729	0.900
LFINF/H:3	Sa at 1.0 s	-2.112	0.516	-0.895	0.635	-0.353	0.633	0.265	0.623	0.872
LFINF/H:4	Sa at 1.0 s	-2.023	0.465	-0.827	0.589	-0.307	0.617	0.288	0.636	0.899
LFINF/H:5	Sa at 1.0 s	-1.892	0.396	-0.691	0.494	-0.201	0.554	0.415	0.663	0.919
LFINF/H:6	Sa at 1.0 s	-1.759	0.317	-0.564	0.399	-0.080	0.468	0.551	0.601	0.921
LFINF/H:7	Sa at 1.0 s	-1.498	0.297	-0.431	0.396	0.038	0.523	0.653	0.689	0.883
LFINF/H:1/DNO	PGA	-1.126	0.363	-0.330	0.350	-0.119	0.331	0.162	0.400	0.969
LFINF/H:2/DNO	Sa at 0.3 s	-0.875	0.328	0.036	0.384	0.375	0.513	0.872	0.602	0.922
LFINF/H:3/DNO	Sa at 1.0 s	-2.501	0.456	-1.607	0.505	-1.142	0.486	-0.587	0.502	0.928
LFINF/H:4/DNO	Sa at 1.0 s	-2.401	0.362	-1.400	0.430	-0.981	0.444	-0.402	0.548	0.952
LFINF/H:5/DNO	Sa at 1.0 s	-2.112	0.329	-1.184	0.362	-0.828	0.452	-0.323	0.486	0.939
LFINF/H:6/DNO	Sa at 1.0 s	-2.037	0.304	-1.087	0.377	-0.690	0.505	-0.199	0.456	0.926
LFINF/H:7/DNO	Sa at 1.0 s	-1.996	0.342	-1.039	0.443	-0.588	0.612	0.025	0.702	0.910
LWAL/H:5	Sa at 1.0 s	-1.241	0.524	-0.524	0.715	-0.180	0.733	0.262	0.693	0.877
LWAL/H:6	Sa at 1.0 s	-1.053	0.418	-0.320	0.574	-0.004	0.557	0.403	0.516	0.917
LWAL/H:7	Sa at 1.0 s	-1.005	0.323	-0.349	0.441	-0.056	0.442	0.335	0.454	0.949
LWAL/H:8	Sa at 1.0 s	-0.816	0.294	-0.260	0.361	-0.012	0.391	0.371	0.490	0.963
LWAL/H:9	Sa at 1.0 s	-0.776	0.287	-0.219	0.355	0.037	0.408	0.434	0.527	0.961
LWAL/H:10	Sa at 1.0 s	-0.748	0.317	-0.188	0.380	0.079	0.452	0.506	0.593	0.946

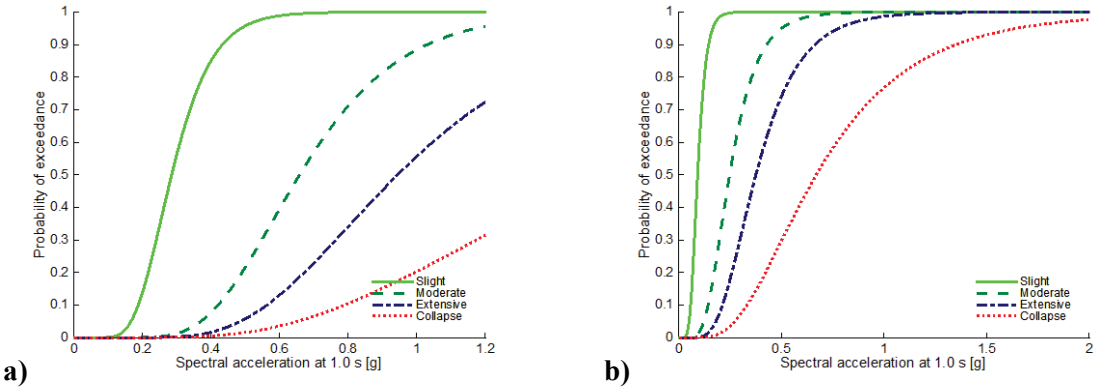

Figure 8. Fragility curves for a) LFM/DUC/H:4 and b) LFINF/H:4/DNO

Table 10. Fragility functions for wooden and unknown building classes.

Typology	IM	Damage States								Mean R
		Slight		Moderate		Extensive		Collapse		
		λ	x	λ	x	λ	x	λ	x	
W+WLI/H:1	Sa at 0.3 s	0.107	0.403	0.853	0.450	1.144	0.449	1.594	0.573	0.937
W+WLI/H:2	Sa at 0.3 s	0.151	0.323	0.857	0.350	1.202	0.484	1.781	0.712	0.910
UNK	Sa at 0.3 s	-0.877	0.360	-0.143	0.401	0.151	0.362	0.489	0.378	0.976

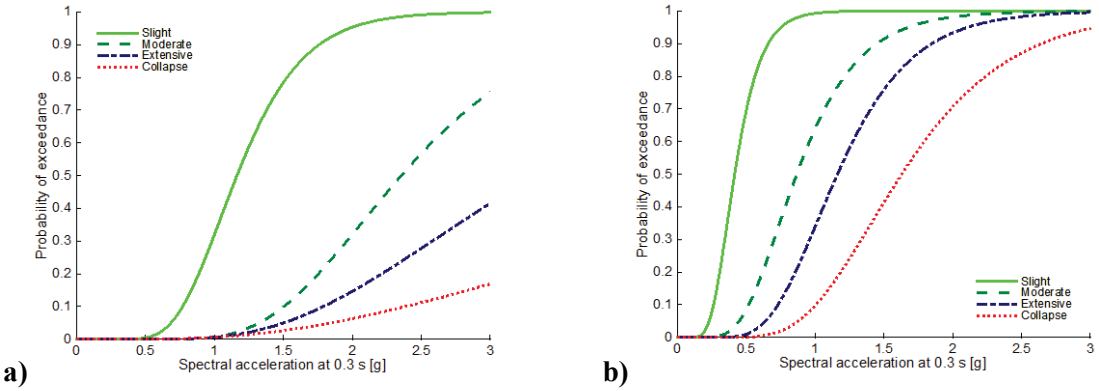

Figure 9. Fragility curves for a) W+WLI/H:2 and b) UNK

CONCLUSIONS

This study presented the development of a uniform fragility model for 54 building classes in the Andean countries. Each fragility function was derived based on the seismic performance of 150 SDOF oscillators when subjected to a set of 300 ground motion records. The structural capacity for each building class was defined based on existing fragility and vulnerability

studies, discussions from two workshops organized locally, and expert judgement of several practitioners from the region. Different ductility levels, damage schemes, and response behaviours were considered, depending on the building class. Each fragility function was modelled using a cumulative lognormal distribution, and the representative intensity measure level was selected based on the correlation between ground shaking and damage distribution. All of these fragility functions are publicly available through the GEM Vulnerability Database (Yepes *et al*. 2016) at the OpenQuake-platform (http://platform.openquake.org).

Despite the usefulness of these models, it is important to acknowledge their limitations and range of applicability. These fragility functions do not capture the specific features of the building stock at the local level. For the assessment of earthquake losses at a local scale, models derived using a more detailed methodology and considering the local characteristics of the building stock should be considered.

ACKNOWLEDGEMENTS

The authors would like to thank the SwissRe Foundation for the financial support of the SARA Project, as well as Suramericana insurance company for the technical guidance and assistance in the preparation of the workshops. The authors are also grateful for the feedback provided by the local experts that participated in the workshops in Lima and Medellin.

REFERENCES

Ahmad N, Crowley H, Pinho R, Ali Q (2011). Seismic Risk Assessment and Loss Estimation of Building Stock of Pakistan. *PhD Thesis,* ROSE School, IUSS Pavia.

Akkar S, Sucuoğlu M, Yakut A (2005). Displacement-Based Fragility Functions for Low- and Mid-rise Ordinary Concrete Buildings. *Earthquake Spectra*, 21(4):901-927.

Applied Technology Council (ATC-40) (1996). Seismic Evaluation and Retrofit of Concrete Buildings. *Report ATC-40*, Redwood City, California.

Bal, I.E., Crowley, H., Pinho, R., Gulay, FG. (2008). Detailed Assessment of Structural Characteristics of Turkish RC Building Stock for Loss Assessment Models. Soil Dyn. and Earth. Eng., 28:914-932.

Bal, I.E., Crowley, H., Pinho, R. (2010). Displacement-based earthquake loss assessment: Method development and application to Turkish building stock. ROSE Research Report 2010/02, IUSS Press, Pavia, Italy.

Bonett, R. (2003). Vulnerabilidad y riesgo sísmico de edificios. Aplicación a entornos urbanos en zonas de amenaza alta y moderada. *Doctoral Thesis*, Universidad Politécnica de Cataluña.

Borzi, B., Crowley, H., Pinho, R. (2008). Simplified Pushover-Based Earthquake Loss Assessment (SP-BELA) Method for Masonry Buildings. *International Journal of Architectural Heritage*, Vol. 2, No. 4, pp. 353-376.

Brzev S., C. Scawthorn, A.W. Charleson, L. Allen, M. Greene, K. Jaiswal, and V. Silva (2013). GEM Building Taxonomy Version 2.0, GEM Technical Report 2013-02 V1.0.0, 188 pp., GEM Foundation, Pavia, Italy, doi: 10.13117/GEM.EXP-MOD.TR2013.02

Calvi, G.M. (1999). A Displacement-Based Approach for Vulnerability Evaluation of Classes of Buildings. *Journal of Earthquake Engineering*, 3(3):411-438.

Camelo, V. (2003). Dynamic Characteristics of Woodframe Buildings. *Doctoral Thesis*, California Institute of Technology.

Casotto, C. (2016). Damage-dependent fragility assessment: critical issues and recommendations. *Doctoral Thesis,* IUSS Pavia, Italy.

Crowley, H., Pinho, R. (2004a). Period-Height Relationship for Existing European Reinforced Concrete Buildings. *Journal of Earthquake Engineering*, 8(1):93-119.

Crowley, H., Pinho, R., Bommer, J. (2004b) A Probabilistic Displacement-based Vulnerability Assessment Procedure for Earthquake Loss Estimation. *Bulletin of Earthquake Engineering*, 2(2): 173-219.

Crowley, H., Pinho, R. (2006). Simplified Equations for Estimating the Period of Vibration of Existing Buildings. *First European Conference on Earthquake Engineering and Seismology*. Geneva, Switzerland.

D'Ayala, D., Meslem, A., Vamvatsikos, D., Porter, K., Rossetto, T., Crowley, H., Silva, V. (2014). Guidelines for Analytical Vulnerability Assessment of Low-Mid-Rise Buildings – Methodology. Vulnerability Global Component Project, GEM Foundation, Pavia, Italy.

Delgado, R., Rodríguez, C. (2006). Edificios peruanos con muros de concreto de ductilidad limitada. *Undergraduate Thesis*. Pontificia Universidad Católica del Perú.

Dolan, J.D. (1989). The Dynamic Response of Timber Shear Walls. *Doctoral Thesis*, University of British Columbia.

Erberik, M. (2007). Fragility-based assessment of typical mid-rise and low-rise RC buildings in Turkey. *Engineering Structures*, 30:1360-1374.

Federal Emergency Management Agency - FEMA (2009). FEMA P695. Quantification of Building Seismic Performance Factors. Prepared by Applied Technology Council for the FEMA. Washington, D.C., USA.

Gamba P. (2014). Global Exposure Database: Scientific Features, GEM Technical Report 2014-10 V1.0.0, 46 pp., GEM Foundation, Pavia, Italy, doi: 10.13117/GEM.EXP-MOD.TR2014.10

Ghobarah, A. (2004). On Drift Associated with Different Damage Levels. Performance-Based Seismic Design: Concepts and Implementation, Ljubljana, Slovenia.

Goda, K. (2014). Record selection for aftershock incremental dynamic analysis. *Earthquake Engineering and Structural Dynamics*, 44(7):1157-1162.

Gómez, I., Rodríguez, E. (2006) "Generación de funciones de vulnerabilidad para edificaciones de mampostería no reforzada de baja altura utilizando técnicas de simulación", Uni. Industrial de Santander, Colombia.

Haindl M., Hube M.A., Arteta C. (2015). Seismic performance assessment of a reinforced concrete shear wall house. *VII Congreso Nacional de Ingeniería Sísmica*, Bogotá, Colombia.

Ibarra, L.F., Krawinkler, H. (2005). Global Collapse of Frame Structures under Seismic Excitations. Final Report on PEER Project 3192002. The John A. Blume Earthquake Engineering Center, Stanford, California, USA.

Jaiswal, K., Petersen, M., Harmsen, S., Smoczyk, G. (2014) "Assessing the Seismic Risk Potential of South America", *Second European Conference on Earthquake Engineering and Seismology*, Istanbul, Turkey.

Lagomarsino, S., Giovinazzi, S. (2006) "Macroseismic and Mechanical Models for the Vulnerability and Damage Assessment of Current Buildings", *Bulletin of Earthquake Engineering*, Vol. 4, No. 4, pp. 415-443.

Maldonado, E., Chio Cho, G. (2009). Estimación de las funciones de vulnerabilidad sísmica en edificaciones en tierra. *Ingeniería y Desarrollo*, 25: 180-199.

Maldonado, E., Jasbón, N., Chio Cho, G. (2010). Funciones de vulnerabilidad calculadas para edificaciones para edificaciones en muros de hormigón reforzado. *Rev. Ing. de Construccción*: 25(1):63-82.

Martínez, J. (2012). Caracterización de la vulnerabilidad sísmica utilizando curvas de fragilidad y matrices de probabilidad de daño para algunas tipologías estructurales de hormigón armado. Aplicación a la ciudad de Valdivia, Región de Los Ríos. *Undergraduate Thesis*, Universidad Austral de Chile.

McKenna, F., Fenves, G. L., Scott, M. H., and Jeremic, B., (2000). Open System for Earthquake Engineering Simulation (OpenSees). Pacific Earthquake Engineering Research Center, Uni. of California, Berkeley.

Milutinovic, Z.V., Trendafiloski, G.S. (2003). WP4: Vulnerability of Current Buildings. Risk-UE Project Handbook. *RISK-UE Project Report*

Olbrich, F. (2015). Evaluación sismorresistente de edificaciones patrimoniales de mampostería no reforzada ubicadas en el Área Metropolitana de Caracas. *Master Thesis*, Universidad Central de Venezuela.

Oliveira, C., Navarro, M. (2010). Fundamental Periods of Vibration of RC Buildings in Portugal from In-Situ Experimental and Numerical Techniques. *Bulletin of Earthquake Engineering*, 8(3):609-642

Pagani, M., Monelli, D., Weatherill, G., Danciu, L., Crowley, H., Silva, V., Henshaw, P., Butler, L., Nastasi, M., Panzeri, L., Simionato, M., Vigano, D. (2014) "OpenQuake-Engine: An Open Hazard (and Risk) Software for the Global Earthquake Model", *Seismological Research Letters*, 85(3):692-702.

Quintanilla, E. and Ruiz, K. (2011). Estudio del comportamiento dinámico de una muestra de estructuras de mampostería. *Undergraduate Thesis*, Universidad Industrial Santander

Quiroz, L., Maruyama, Y. (2013). Comparison of numerical fragility curves for thin RC walls used in Lima, Peru considering variations of ground motion datasets. *Proceedings of the 13th East Asia-Pacific Conference on Structural Engineering and Construction*, Sapporo, Japan.

Quiroz, L., Maruyama, Y. (2014). Fragility functions and seismic performance of Peruvian thin RC wall buildings. *10th U.S. National Conference on Earthquake Engineering*, Anchorage, Alaska.

Rojas, R. (2010). Curvas de fragilidad sísmica para edificios aporticados de concreto reforzado de poca altura. *Undergraduate Thesis*, Universidad Central de Venezuela.

Rojas, R., Coronel D. G. (2014). Curvas de fragilidad y vulnerabilidad sísmica del edificio residencial tipo 6m8-66 mediante análisis estático no lineal. *Jornada de Investigación de la Facultad de ingeniería (JIFI), Universidad Central de Venezuela*, Caracas, Venezuela.

Rossetto T., Ioannou I., Grant D.N. (2013). Existing empirical fragility and vulnerability functions: Compendium and guide for selection, GEM Technical Report, GEM Foundation, Pavia, Italy.

Safina, S. (2003). Propuesta preliminar de funciones de daño para las principales categorías de edificaciones de la ciudad de Caracas. *Report*, Caracas, Venezuela.

Safina, S., Andrade, M., Schmitz, M., Jraige, C., Espinosa, L. (2008). Seismic Response of Reinforced Concrete Buildings in Caracas, Venezuela. *14th World Conf. on Earthquake Engineering*, Beijing, China.

Salgado-Gálvez, M.A., Zuloaga-Romero, D., Bernal, G.A., Mora, M.G., Cardona, O.D. (2014). Fully probabilistic seismic risk assessment considering local site effects for the portfolio of buildings in Medellín, Colombia. *Bulletin of Earthquake Engineering*, 12(2):671-695.

Silva, V., Crowley, H., Pinho, R., Varum, H. (2013b). Extending Displacement-Based Earthquake Loss Assessment (DBELA) for the Computation of Fragility Curves. *Eng. Structures*, 56: 343-356

Silva, V., Crowley, H., Varum, H., Pinho, R., Sousa, L. (2014a). Investigation of the Characteristics of Portuguese Regular Moment-Frame RC Buildings and Development of a Vulnerability Model. *Bull. of Earthquake Engineering*.

Silva, V., Crowley, H., Varum, H., Pinho, R., Sousa, R. (2014b). Evaluation of Analytical Methodologies Used to Derive Vulnerability Functions. *Earthquake Engineering and Structural Dynamics,* 43(2):181-204.

Silva, V., Crowley, H., Bazzurro, P. (2015a). Exploring Risk-Targeted Hazard Maps for Europe. *Earthquake Spectra*, under review

Silva, V., Casotto, C., Rao, A., Villar, M., Crowley, H. and Vamvatsikos, D. (2015b). OpenQuake Risk Modeller's Toolkit - User Guide. Global Earthquake Model. *Technical Report* 2015-09

Tapia, P., Roldán, W., Villacis, C. (2002). Vulnerabilidad sísmica de las ciudades del norte de Chile: Arica, Antofagasta y Copiapó. *VIII Jornadas Chilenas de Sismología e Ing. Antisísmica*, Valparaíso.

Tarque, N. (2008). Seismic Risk Assessment of Adobe Dwellings. *Master Thesis*, European School for Advanced Studies in Reduction of Seismic Risk (ROSE School), University of Pavia, Italy.

Tarque, N., Crowley, H., Pinho, R., Varum, H. (2012). Displacement-Based Fragility Curves for Seismic Assessment of Adobe Buildings in Cusco, Peru. *Earthquake Spectra*, 28(2): 759-794.

Varum, H., Tarque, N., Silveira, D., Camata, G., Lobo, B., Blondet, M., Figueiredo, A., Rafi, M., Oliveira, C., Costa, A. (2014). Structural Behaviour and Retrofitting of Adobe Masonry Buildings. *Structural Rehabilitation of Old Buildings*, Building Pathology and Rehabilitation, Vol. 2, Springer-Verlag Berlin Heidelberg.

Vásquez, L., Hernández, G., Campos, R., González, M. (2012). Caracterización mecánica de muros estructurales de madera. *Technical Report No. 191*, Instituto Forestal, Bío Bío, Chile.

Velásquez, J. (2006). Estimación de pérdidas por sismo en edificios peruanos mediante curvas de fragilidad analíticas. *Undergraduate Thesis*, Pontificia Universidad Católica del Perú.

Vielma, J. C., Alfaro A., Barrios A. (2014). Determinación de curvas de fragilidad mediante análisis incremental dinámico. *Revista Sul-Americana de Engenharia Estrutural*, *Passo Fundo*, 11(1): 135-154.

Watson-Lamprey, J. and Abrahamson, N. (2006). Selection of ground motion time series and limits on scaling. *Soil Dynamics and Earthquake Engineering*, 26: 477-482.

Yepes-Estrada, C., Silva, V., Valcárcel, J., Acevedo, A., Hube, M., Coronel, G. (2015). A Uniform Residential Building Inventory for South America. *Earthquake Spectra*, under review.

Yepes C, Silva V, Rossetto T, D'Ayala D, Ioannou I, Meslem A, Crowley H (2016). The Global Earthquake Model Physical Vulnerability Database. Earthquake Spectra.